Microfluidics and Nanofluidics (2019) 23:83
https://doi.org/10.1007/s10404-019-2242-x

RESEARCH PAPER

Dynamic particle ordering in oscillatory inertial microfluidics

Claudius Dietsche[1,2] · Baris R. Mutlu[1] · Jon F. Edd[1,3] · Petros Koumoutsakos[2] · Mehmet Toner[1,4]

Received: 6 February 2019 / Accepted: 15 April 2019 / Published online: 22 May 2019

Abstract
Particles suspended in conduit flows at small and intermediate Reynolds numbers cluster on specific focal positions while also forming particle pairs and trains due to flow-mediated interactions. The recent introduction of oscillatory inertial microfluidics has enabled the creation of virtually infinite channels, allowing the manipulation of particles at extremely low particle Reynolds numbers ($Re_p \ll 1$). Here, we investigate experimentally the dynamics of formation, the robustness and the stability of particle pairs, and the precision of the inter-particle distance in an oscillatory flow field, in microchannels with a rectangular cross section. Our results indicate that the cross-sectional arrangement of the particles is fundamental in determining the characteristics of the resulting particle pair.

Keywords Microfluidics · Oscillatory flow · Inertial focusing · Train of particles · Hydrodynamic self-assembly

1 Introduction

Particles in confined, finite Reynolds number ($\sim 1 < Re < \sim 1000$) flows exhibit lateral focusing and longitudinal ordering patterns. This behavior is utilized for label-free cell manipulation and organization in numerous biomedical systems, and is widely known as inertial microfluidics. In inertial microfluidics, cells experience forces lateral to their flow direction, which lead to stable and precise equilibrium positions in the cross section of the channel (Segré and Silberberg 1961; Di Carlo et al. 2007; Martel and Toner 2014). The location of the equilibrium positions is affected by the particle Reynolds number ($Re_P = Ua^2/\nu D_h$, where U is the characteristic velocity of the fluid, a is the particle diameter, ν is the kinematic viscosity, and D_h is the hydraulic diameter of the channel), the three-dimensional geometry of the channel, and the particle diameter (Di Carlo et al. 2009; Yuan et al. 2018; Mukherjee et al. 2019). This precise particle and cell ordering is exploited in various applications such as cell separation and enrichment (Fachin et al. 2017; Syed et al. 2017; Kim et al. 2018), rare cell isolation (Ozkumur et al. 2013; Shen et al. 2014), and cell-bead co-encapsulation (Lagus and Edd 2013a; Moon et al. 2018).

In addition to focusing, particles self-assemble into longitudinal pairs and trains via flow-mediated interactions (Lee et al. 2010). The perturbed Poiseuille flow around a particle is reflected at the channel walls which results in a secondary flow that is largely responsible for the particles' interactions and their consequential longitudinal organization (Matas et al. 2004; Humphry et al. 2010; Lee et al. 2010; Pan et al. 2018). At sufficiently high concentrations, particles form coherent trains with equivalent inter-particle distances (Matas et al. 2004; Humphry et al. 2010; Lee et al. 2010; Kahkeshani et al. 2015; Gao et al. 2017; Del Giudice et al. 2018). However, if the concentration is further

This article is part of the topical collection "Particle motion in non-Newtonian microfluidics" guest edited by Xiangchun Xuan and Gaetano D'Avino.

Claudius Dietsche and Baris R. Mutlu contributed equally to this work.

✉ Claudius Dietsche
claudius.dietsche@gmail.com

Petros Koumoutsakos
petros@ethz.ch

Mehmet Toner
mtoner@hms.harvard.edu

[1] BioMEMS Resource Center, Center for Engineering in Medicine and Surgical Services, Massachusetts General Hospital, Harvard Medical School, Boston, MA 02114, USA

[2] Computational Science and Engineering Laboratory, ETH Zürich, Clausiusstrasse 33, 8092 Zurich, Switzerland

[3] Massachusetts General Hospital Cancer Center, Harvard Medical School, Boston, MA 02114, USA

[4] Shriners Hospitals for Children, Boston, MA 02114, USA

increased, the focusing of particles is impaired and no stable train can be formed (Kahkeshani et al. 2015; Reece and Oakeya 2016; Gupta et al. 2018). The presence of unevenly spaced or unstable trains is detrimental to various biomedical applications which rely on precise cell ordering (Edd et al. 2008; Di Carlo 2009; Hur et al. 2010; Lagus and Edd 2012, 2013b). Therefore, precise determination of particle ordering is of significant theoretical and practical interest.

Oscillatory inertial microfluidics is a recent technique which enables inertial focusing at extremely low particle Reynolds number flows, and can be used to manipulate submicron-scale particles and bacteria (Mutlu et al. 2018). The method relies on switching the direction of the flow field at a sufficiently high frequency, such that the suspended particles travel distances which are significantly (i.e, orders of magnitude) longer than the finite length of the microchannel. As inertial lift forces are independent of the flow direction, the particles focus to the same position regardless of the flow direction. Furthermore, this method also enables continuous observation of particles during their inertial focusing and longitudinal ordering process, which is extremely useful for making extended observations without sacrificing spatial resolution.

In this study, we investigated the dynamic formation, the precision and the stability of particle pairs and trains in an oscillatory inertial microfluidics system. We observed that the magnitude of the particle–particle interactions and the stability of the resulting pairs are significantly affected by the cross-sectional geometric arrangement of the particle pair. Focused particles attracted, repelled, or minimally interacted with each other based on their geometric arrangement and the inter-particle distance. We identified different regimes of particle interactions with respect to particle concentration, based on theoretical limitations and experimental findings. Consequently, we developed and experimentally verified a correlation between the inter-particle distance and the concentration of the particles. We identified the ratio between the short dimension of the channel and the particle size as the determining parameter in particle spacing, and proposed a correlation to estimate the inter-particle distance which we also experimentally verified.

2 Experimental procedure

The oscillating flow was generated by two three-way valves from the Lee Company (LHDA 0533315H) each connected by Tygon tubing (ID: 0.02″, OD: 0.06″, Cole Palmer) to a compressor, the microfluidic device, and the atmosphere (sink), as previously reported by Mutlu et al. (2018) (Fig. 1a). A high-speed camera (Phantom v4.2, Vision Research) was used to record images of the suspended

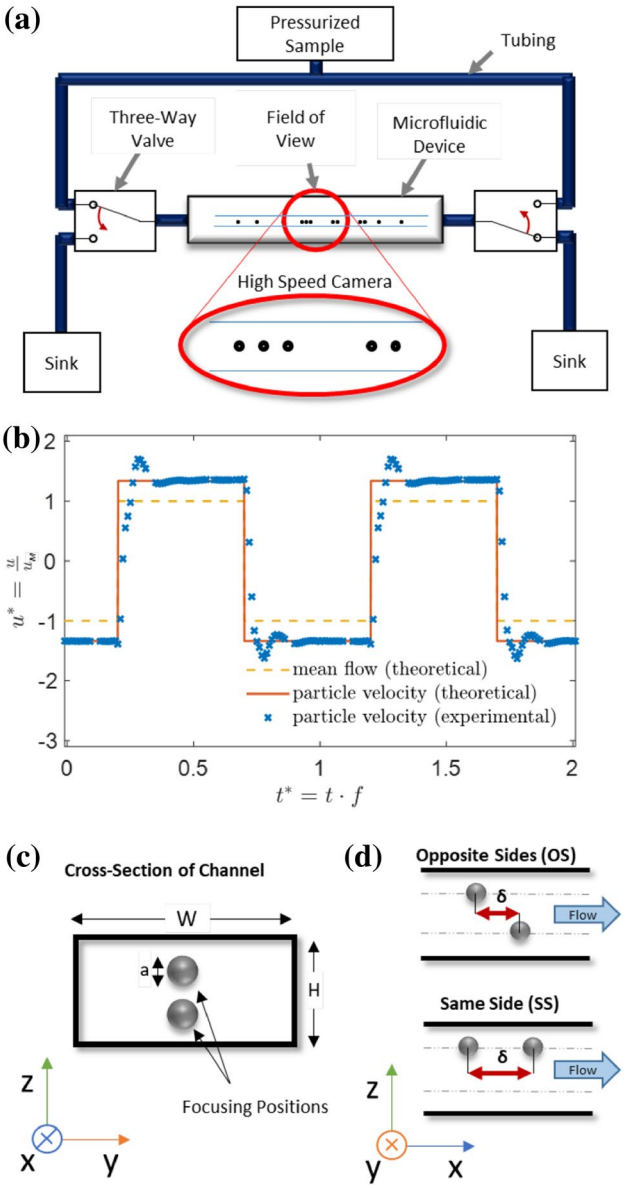

Fig. 1 **a** Two three-way solenoid valves were connected via a Tygon tubing to the pressurized sample, the microfluidic device, and the sink. In the microfluidic device, the suspension of particles was oscillated. **b** Typical particle velocity profile (u) was measured and normalized by the mean flow velocity [$u_M = p/(R_h A)$, where R_h is the hydraulic resistance, A is the channels' cross-sectional area, and p is the applied pressure]. The dashed line depicts the mean flow profile $u_P = u_M$ sgn[sin($2\pi tf$)] normalized by u_M over two oscillations. The theoretical particle velocity ($u_T \approx 1.34\ u_M$, solid line) is greater than the velocity of the mean flow due to their focusing position. **c** Focusing positions in the cross section of a microchannel are shown. **d** Depending on the particles focal position two distinct pair arrangements exist. Particles occupying the same focal side (SS) or opposing focal sides (OS)

monodispersed particles ($\rho = 1.05$ g/cm^3, $a = 3$–20 μm) via a microscope (Eclipse 90 i, Nikon) equipped with a 10× and 20× magnification. The particles from Thermo Scientific

(Fluoro-Max) were suspended at volume concentrations (c_v) of $0.0001 < c_v < 0.02$ in phosphate buffered saline and density matched with OptiPrep (Sigma-Aldrich). The different devices were fabricated using standard soft lithography (Duffy et al. 1998) with the following dimensions: Device A had a length $L = 3$ cm, a width $W = 40$ μm, and a height $H = 24$ μm (in short: $3 \times 40 \times 24$). Devices B–E had the dimensions $3 \times 80 \times 24$, $6 \times 40 \times 29$, $3 \times 130 \times 40$, and $3 \times 130 \times 80$, respectively. The ratio between the width (W) and the height (H) of all channels was greater than 1.4 to guarantee focusing of the particles to two focusing positions (instead of fours in a squared channel).

The frequency of the oscillation (f) was selected, such that the travel distance of particles during an oscillation is smaller than half of the channel length ($f > 2\ u/L$, where u is the average velocity of the particles). This led to frequencies between $f = 2$ Hz and $f = 10$ Hz, and ensured that the particles observed during a measurement stayed inside the microfluidic channel. In this frequency range, the particles experienced a strain per oscillation ($S = L/H$) in the range of $375 < S < 2000$ and the system had a Womersley number $[\alpha = D_h(2\pi f/\nu)^{1/2}]$ in the range $0.1 < \alpha < 0.8$. These parameters indicate that a full velocity profile is established during every oscillation and that the flow can be treated as unidirectional (Loudon and Tordesillas 1998; Morris 2001). Therefore, the oscillation frequency range of this study is expected to have no effect on the dynamic particle pair formation and inter-particle distance, which was also verified experimentally. The particle velocity profile in each oscillation (Fig. 1b) was consistent with the theoretical velocity of inertially focused particles (Di Carlo et al. 2009).

At the initialization of the experiments, the particle suspension was oscillated in the microfluidic channel until all particles inertially migrated to one of the two focus positions (Fig. 1c). Due to the rectangular channel geometry, adjacent particles in the longitudinal direction could have only two geometric arrangements based on occupied focus positions: (1) same side (SS) and (2) opposite sides (OS) (Fig. 1d). The inter-particle distance (δ) was measured from center-to-center of adjacent particles and was normalized by the particle diameter ($\delta^* = \delta/a$) (Matas et al. 2004; Humphry et al. 2010; Kahkeshani et al. 2015; Gao et al. 2017). The normalized inter-particle distances of particle pairs in the SS and OS arrangements are denoted as ${}^{SS}\delta^*$ and ${}^{OS}\delta^*$, respectively.

3 Results and discussion

We observed that the dynamics of pair formation differed significantly based on the pair's geometric arrangement (SS or OS). Pairs in OS arrangement, pair formation occurred rapidly when the non-dimensional inter-particle distance (δ^*) reached a critical value (Fig. 2a). After

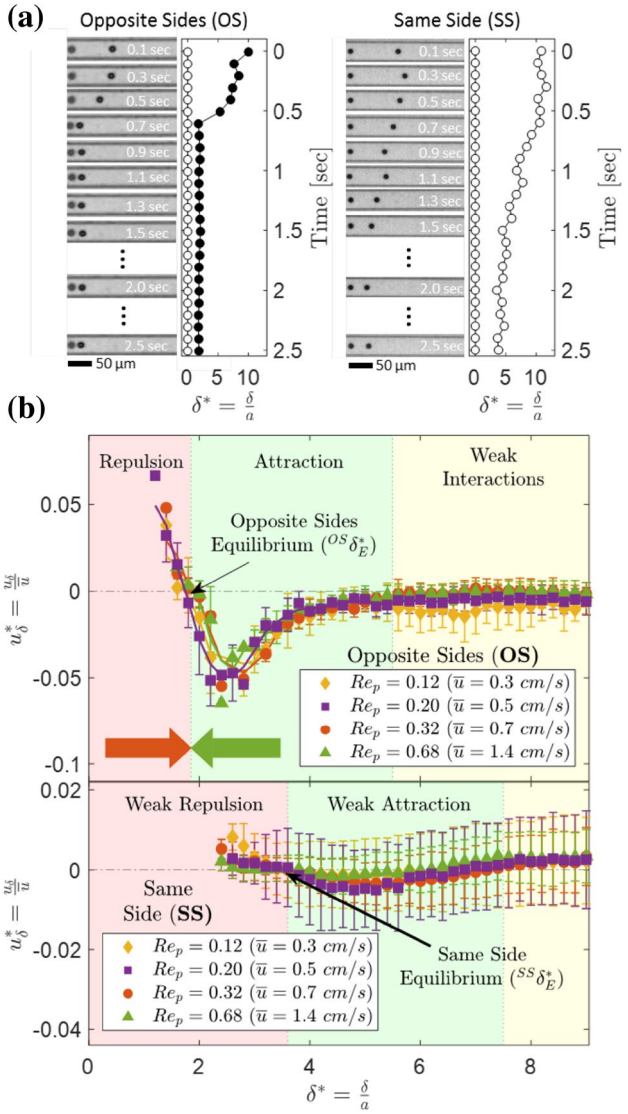

Fig. 2 **a** High-speed images of two particle pairs are shown. Their corresponding normalized inter-particle distance ($\delta^* = \delta/a$) is plotted against the time. The shade of the marker indicates the focusing side of the particle. **b** Initial attraction and repulsion of particle pair formation was investigated with the non-dimensional relative velocity ($u^*_\delta = u_\delta/\bar{u}$) as a function of δ^*. The solid lines on OS represent a moving average of the data values. The error bars indicate the standard deviation of multiply observed particle pairs. The experiments were conducted with $a = 10$ μm particles in device A with a cross section of 40×24 μm^2

formation, spacing was robust as the ${}^{OS}\delta^*$ remained constant with diminutive fluctuations. In contrast, pair formation occurred more gradually in the SS arrangement, and ${}^{SS}\delta^*$ was subject to substantial fluctuations after pair formation. To better illustrate this phenomenon, we calculated the relative velocity of particles in a pair ($u_\delta = d\delta/dt$). A negative u_δ signifies that particles are moving closer and a positive u_δ indicates that they are moving apart. The non-dimensional relative velocity (u^*_δ) was calculated by

dividing u_δ by the average velocity ($\bar{u}$= (u_1+u_2)/2). Independent of the pair arrangement, particles below a certain inter-particle distance ($^{OS}\delta^* < 1.8$ and $^{SS}\delta^* < 3.7$) moved away from each other (Fig. 2b, $u_\delta^* > 0$). At intermediate δ^* ($1.8 < {}^{OS}\delta^* < 5.5$ and $3.7 < {}^{SS}\delta^* < 7$), particles in a pair moved towards each other ($u_\delta^* < 0$). At higher δ^*, particles in both pair arrangements minimally interacted ($u_\delta^* \approx 0$). Note that the magnitude of u_δ^* of pairs in OS arrangement was an order of magnitude greater than in the SS arrangement.

The sign and magnitude of the non-dimensional relative velocity (u_δ^*) indicate the nature and the scale of the particle interactions. A $u_\delta^* > 0$ signifies that the particles in a pair move apart and thus exhibit repulsive interactions. In contrast, $u_\delta^* < 0$ means that particles approach each other and exhibit attractive interactions. Both pair arrangements exhibited repulsive interactions at small δ^* (Fig. 2b), and the magnitude of these repulsive interactions increased when particles got closer (i.e., δ^* got smaller). At intermediate δ^*, particle pairs showed an attractive interaction. The interplay between attractive and repulsive interactions led to an equilibrium distance (δ_E^*) between pairs at which u_δ^* was zero. For particles in OS arrangement, the strong interactions led to a robust equilibrium at $^{OS}\delta_E^* = 1.8$, whereas the weak interactions in SS arrangement led to a weak equilibrium at $^{SS}\delta_E^* \approx 3.7$. At higher δ^*, both pair arrangements exhibited weak interactions that were neither unambiguously repulsive nor attractive.

Our results showed that the particle–particle interactions (as measured by u_δ^*) correlate linearly with the flow velocity (U), and may impair the inertial focusing of particles at sufficiently low flow velocities. We observed that u_δ^* stayed constant when U was increased to adjust Re_p from 0.1 to 0.7 (Fig. 2b). This is only possible if u_δ is linearly correlated with U, due to the mathematical definition of u_δ^* ($=u_\delta/\bar{u}$). Consequentially, for constant fluid properties and a fixed geometry, particle–particle interactions correlate linearly with Re_p, whereas the lateral drift velocity induced by inertial lift forces correlate with U^2 and thus Re_p^2 (Di Carlo et al. 2007). In Stokes flow, the secondary flow around a single particle is linearly correlated with the rotational velocity of the particle, which is linearly correlated with the flow velocity (U) (Mikulencak and Morris 2004). The inertia of the flow only marginally affects the secondary flow around a single particle in a parabolic channel flow (Mikulencak and Morris 2004; Lee et al. 2010). Therefore, we postulate that particle–particle interactions correlate with the secondary flow and are predominantly unaffected by the inertia of the fluid. This indicates that when the flow velocity (U) decreases, particle–particle interactions diminish less compared to inertial lift forces, which may eventually impair the focusing and ordering behavior of particles. In our experimental setup, we observed defocusing of particles at flow velocities below $U < 0.1$ cm/s ($a = 10$ µm in device A); however, further studies are needed to investigate these critical flow velocities.

We observed that the stability of pairs and the precision of the ordered particle spacing (δ^*) also differed significantly between the two particle arrangements (i.e., OS and SS). The concentration of inertially focused particles in a rectangular microchannel was described by the line concentration $c_L = aN/L_F$ (Di Carlo 2009), where a is the particle diameter, L_F is the length of the field of view and N is the number of particles within the field of view. δ^* was analyzed by the probability distribution of δ^* [$p(\delta^*)$] at different c_L. Particles in OS arrangement formed precisely spaced pairs and were minimally affected by c_L. This can be seen at high and narrow $p(\delta^*)$ peaks over a wide c_L range (Fig. 3a). In contrast, pair spacing in the SS arrangement was significantly affected by c_L, which can be seen by the shift of $p(\delta^*)$ with an increase in c_L. An increase in c_L led to a decrease in the spread of $p(\delta^*)$ and an increase in the maximum $p(\delta^*)$. We defined δ_P^* as δ^* with the highest probability [peak value of $p(\delta^*)$] at a specific c_L. The most probable normalized inter-particle distance in the OS arrangement ($^{OS}\delta_P^*$) was in good agreement with the OS equilibrium distance ($^{OS}\delta_E^*$, see Fig. 2b) at $^{OS}\delta_P^* = {}^{OS}\delta_E^* = 1.8$ (Fig. 3b, closed diamonds). In contrast for SS pairs, $^{SS}\delta_P^*$ was initially higher than $^{SS}\delta_E^*$, but progressively decreased with an increase in c_L until $^{SS}\delta_P^* = {}^{SS}\delta_E^* = 3.7$ at $c_L = 0.22$ (Fig. 3b, open diamonds). At higher c_L values, both pair arrangements showed the same downwards trend in δ_P^* with an increase in c_L. For both arrangements, their δ_P^* values were below the respective equilibrium positions.

At high line concentrations (c_L), we found that the normalized inter-particle distance (δ^*) is directly correlated with c_L. An equally spaced train with N particles has a length of

$$L_t = (N-1)a\delta^*. \quad (1)$$

The line concentration of this train is given by

$$c_L = (N-1)a/L_t. \quad (2)$$

The equations resolved for δ^* result in the geometrical dependency $\delta^* = 1/c_L$ which describe a saturation limit (Fig. 3b). For a train of equally spaced particles, δ_P^* above the saturation limit is geometrically impossible. At approximately 80% of the saturation limit (80% saturation), $^{SS}\delta_P^*$ is equal to $^{SS}\delta_E^*$. Above the 80% saturation, δ_P^* of both arrangements is equal or smaller than δ_E^* and is eventually influenced by the concentration of particles. Therefore, we define the area between the 80% saturation and the saturation limit as the 'saturated regime' (Fig. 3b, dark shaded area). In this regime, the particle–particle interactions are dominated by repulsive interactions and most particles are part of one coherent particle train. In turn, the strong increase in repulsive interactions for a decrease of δ^* below δ_E^* leads to a very precise δ_P^* in this regime. OS pairs reach an inter-particle

accuracy of up to $\delta^* < 0.1$ ($1 < \mu m$) at $c_L = 0.65$, while SS pairs show a significantly reduced scatter of $p(\delta^*)$ at $c_L = 0.35$ (Fig. 3a). Below the 80% saturation, the low concentration of particles and the interplay of attractive and repulsive interactions prevent the formation of a coherent particle train. This area is defined as 'dilute regime' (Fig. 3b, white area). In this regime, particles on OS form stable particle pairs at ${}^{OS}\delta_P^* = {}^{OS}\delta_E^*$ due to their strong interactions. The weaker interactions between particles on the SS form less stable pairs. They are insufficient to uphold a precise ${}^{SS}\delta_P^*$ at ${}^{SS}\delta_E^*$. This can also be observed at the large spread of $p(\delta^*)$ of SS pairs (Fig. 3a). To negate the influence of the concentration, δ_P^* at 80% saturation is used for the remainder of the study.

We observed an increase in the inter-particle distance (δ_P) with increasing Re_p, over our entire experimental parameter range ($0.01 < Re_p < 1.0$) (Fig. 4). To cover this broad Re_p range, we used differently sized particles ($a = 3$, 5, and 10 µm) in the same channel. In the subrange $0.1 < Re_p < 1.0$, ${}^{OS}\delta_P$ increased only minimally (≈ 2 µm) and ${}^{SS}\delta_P$ stayed approximately constant. This result agrees with our findings in Fig. 2, specifically that the effect of Re_p on δ_E^* is minimal in the Re_p range of $0.1 < Re_p < 0.7$.

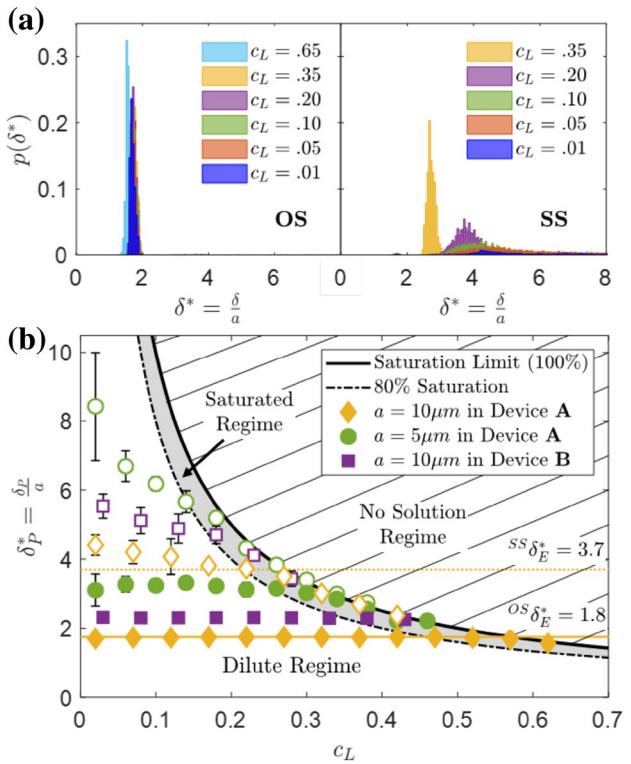

Fig. 3 δ_P is depicted as a function of Re_p for OS pairs (top) and SS pairs (bottom). The dashed line is an exponential least square regression fit to the data values (${}^{OS}\delta_P = -6.4\ Re_p^{-0.16} + 25.3$ µm and ${}^{SS}\delta_P = -3.4\ Re_p^{-0.48} + 40.4$ µm). The error bars indicate the standard deviation of different experiments ($n \geq 3$). The experiments were conducted in device A with a cross section of $40 \times 24\ \mu m^2$

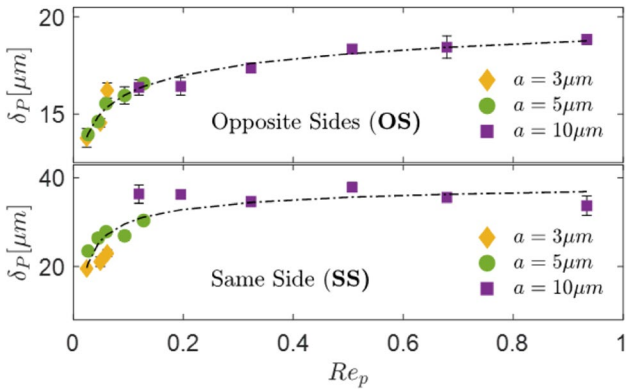

Fig. 4 **a** δ_P of differently sized particles in different channel geometries are depicted. Devices A–E have the dimensions 3 × 40 × 24, 3 × 80 × 24, 6 × 40 × 29, 3 × 130 × 40, and 3 × 130 × 80, respectively. **b** δ_P is depicted as a function of the channel height (H). The equation shown is linear least square regression fits to the data values (dotted lines). Inset: δ_P as a function of the channel width (W). **c** δ_P^* as a function of the non-dimensional channel height ($H^* = H/a$) is depicted for the Re_p range of $0.1 < Re_p < 1$. The equation shown in **b** is least square regression fits to the data values (dotted lines). The results are compared to the works of Humphry et al. 2010, Edd et al. 2008 and Lagus and Edd 2012 (stars). The error bars indicate the standard deviation of different experiments ($n \geq 3$)

We found that the inter-particle distance (δ_P) is linearly correlated with the channel height (H, i.e. the shorter channel dimension), which enabled us to formulate a non-dimensional correlation for δ_P^*. The δ_P of differently sized particles (various a) in various channel geometries were measured (Fig. 5a). The ${}^{OS}\delta_P$ increased from ${}^{OS}\delta_P = 16.4$ µm in channel A ($H = 24$ µm and $a = 10$ µm) to ${}^{OS}\delta_P = 77.9$ µm in channel E ($H = 80$ µm and $a = 10$ µm). The same increase was observed on the SS, where ${}^{SS}\delta_P$ increased from ${}^{SS}\delta_P = 36.4$ µm in channel A ($a = 10$ µm) to ${}^{SS}\delta_P = 121.9$ µm in channel E ($a = 10$ µm). Specifically, the δ_P was linearly correlated to H and minimally influenced by the channel width (W) (Fig. 5b). Varying the particle size (a) in a given channel showed only a minor effect on δ_P compared to the effect of H on δ_P (Fig. 5a). Additionally, the effect of Re_p in the range of $0.1 < Re_p < 1.0$ were also negligible. Based on our results, we fit (least-squares regression) a non-dimensional linear curve to predict ${}^{OS}\delta_P^*$ and ${}^{SS}\delta_P^*$ as a function of the non-dimensional channel height ($H^* = H/a$) as follows: ${}^{OS}\delta_P^* = 1H^* - 0.8$ and ${}^{SS}\delta_P^* = 1.5H^* + 0.2$ (Fig. 5c). In confined channel flows the flow disturbance induced by a particle is reflected by the channel walls and causes the characteristic secondary flow (Zurita-Gotor et al. 2007; Lee et al. 2010). We hypothesize that the linear nature of this reflection is the cause for the linear correlation between the channel height and the inter-particle distance.

Comparison with the previous reports reveal that our results obtained in the oscillatory inertial microfluidic system can also be extended to unidirectional, steady-flow

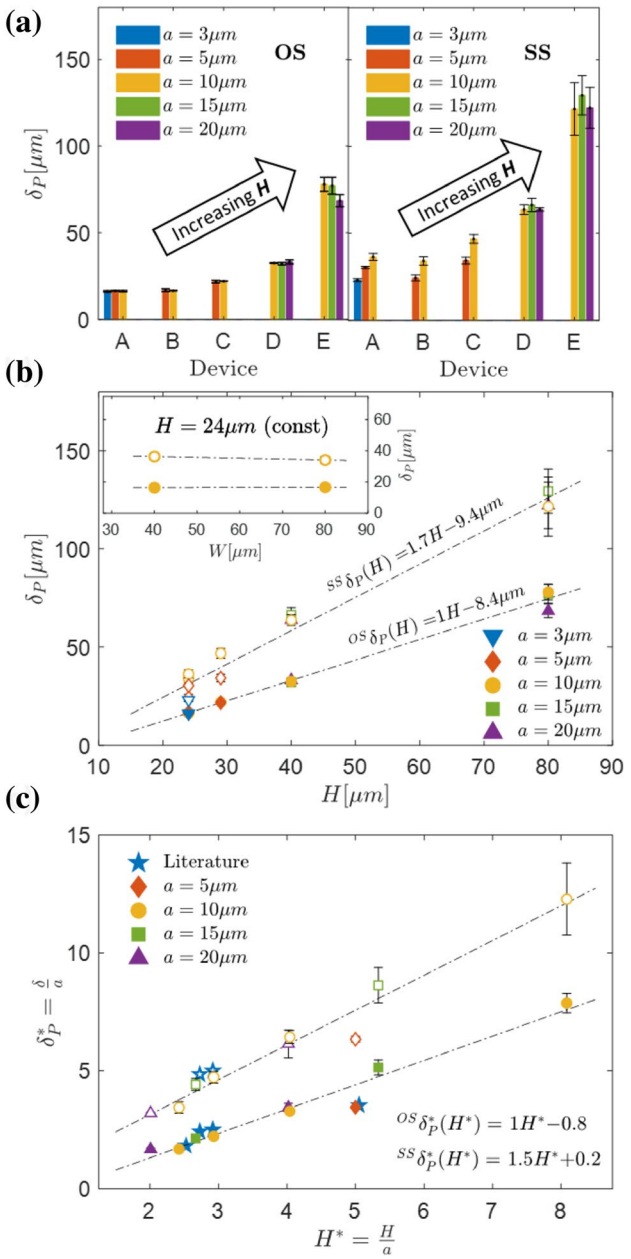

Fig. 5 **a** Probability distribution of the normalized inter-particle distance [$p(\delta^*)$] is formed by measuring δ^* for all particle pairs in every frame, followed by creating a histogram with the obtained data (bin width of 0.5 µm). $p(\delta^*)$ is depicted at different line concentrations (c_L). δ^* with the highest probability [peak value of $p(\delta^*)$] is denoted δ_P^*. **b** δ_P^* of particles on the SS (open) as well as of particles on OS (filled) is depicted. The saturation limit is defined by $\delta^*=1/c_L$. The error bars indicate the standard deviation of different experiments ($n=4$)

inertial microfluidics. The focusing positions and expected particle velocity observed during our measurements are in good agreement with the previously reported inertial, steady-flow focusing positions in rectangular microchannels (Di Carlo et al. 2007, 2009; Lee et al. 2010; Kahkeshani et al. 2015). Furthermore, our inter-particle distance (δ_P) results agree with the results (Fig. 5c, stars) from the previous reports using steady-flow inertial microfluidics (Humphry et al. 2010; Edd et al. 2008; Lagus and Edd 2012). Using an oscillatory flow system, Morris 2001 and Butler et al. 1999 previously demonstrated that particles show the same migration behavior as a unidirectional flow when the strains per oscillations (S) is greater than 1.5. This is consistent with our results, despite the significantly higher range of S ($375 < S < 2000$) investigated in our experiments and the different underlying particle migration physics based on inertial lift forces.

The experimental setup and the method presented in this study could also be used for the investigation of flow focusing dynamics in non-Newtonian fluids. In non-Newtonian fluids such as aqueous viscoelastic solutions, particle-focusing positions switch from the sides of the microchannel to the centerline and to the corners (Yang et al. 2011; D'Avino et al. 2012; Kang et al. 2013). Furthermore, depending on the Reynold's number, inertial forces also contribute to particle migration, resulting in inertia-elastic flow focusing (Lim et al. 2014). We hypothesize that the dynamics of particle ordering will be significantly different than oscillatory inertial microfluidics explored in this study, due to the combined effect of different migration physics and geometrical arrangements of focused particles in non-Newtonian fluids.

4 Conclusion

In summary, we investigated the dynamic formation, the precision, and the stability of particle ordering in an oscillatory inertial microfluidics system, and the extremely low Re_p range enabled by the technique. We quantified the pair interactions based on their geometric arrangement, and determined that pairs in the OS arrangement interact significantly stronger than pairs in the SS arrangement. Consequently, the stronger interactions in the OS arrangement led to more stable, robust, and precisely spaced particle pairs. We determined that the particle–particle interactions correlate linearly with the flow velocity, and postulated that this correlation will lead to impaired inertial focusing and ordering at sufficiently low flow velocities. We identified a saturation limit, and found a geometrical correlation to estimate the inter-particle distance. In addition, we developed a linear correlation between the two non-dimensional parameters: inter-particle distance and channel height (i.e., shorter channel dimension), which can be used to develop applications that rely on precise inter-particle distance of particle trains. Expanding the available parameter space of inertial particle manipulation in terms of particle size and Re_p range has the potential to lead to novel biomedical applications for

smaller bioparticles such as bacteria and exosomes, as well as characterization and phenotyping applications for larger cells. Therefore, we expect that the results of this study will be of significant theoretical and practical interest.

Acknowledgements This work was partially supported by National Institute of Biomedical Imaging and Bioengineering BioMEMS Resource Center Grant P41 EB002503.

References

Butler JE, Majors PD, Bonnecaze RT (1999) Observations of shear-induced particle migration for oscillatory flow of a suspension within a tube. Phys Fluids 11:2865–2877. https://doi.org/10.1063/1.870145

D'Avino G, Romeo G, Villone MM et al (2012) Single line particle focusing induced by viscoelasticity of the suspending liquid: theory, experiments and simulations to design a micropipe flow-focuser. Lab Chip 12:1638–1645. https://doi.org/10.1039/c2lc21154h

Del Giudice F, D'Avino G, Greco F et al (2018) Fluid viscoelasticity drives self-assembly of particle trains in a straight microfluidic channel. Phys Rev Appl 10:1. https://doi.org/10.1103/PhysRevApplied.10.064058

Di Carlo D (2009) Inertial microfluidics. Lab Chip 9:3038–3046. https://doi.org/10.1039/b912547g

Di Carlo D, Irimia D, Tompkins RG, Toner M (2007) Continuous inertial focusing, ordering, and separation of particles in microchannels. Proc Natl Acad Sci 104:18892–18897. https://doi.org/10.1073/pnas.0704958104

Di Carlo D, Edd JF, Humphry KJ et al (2009) Particle segregation and dynamics in confined flows. Phys Rev Lett 102:1–4. https://doi.org/10.1103/PhysRevLett.102.094503

Duffy DC, McDonald JC, Schueller OJA, Whitesides GM (1998) Rapid prototyping of microfluidic systems in poly(dimethylsiloxane). Anal Chem 70:4974–4984. https://doi.org/10.1021/ac980656z

Edd JF, Di Carlo D, Humphry KJ et al (2008) Controlled encapsulation of single-cells into monodisperse picolitre drops. Lab Chip 8:1262–1264. https://doi.org/10.1039/b805456h

Fachin F, Spuhler P, Martel-Foley JM et al (2017) Monolithic chip for high-throughput blood cell depletion to sort rare circulating tumor cells. Sci Rep 7:1–11. https://doi.org/10.1038/s41598-017-11119-x

Gao Y, Magaud P, Baldas L et al (2017) Self-ordered particle trains in inertial microchannel flows. Microfluid Nanofluid 21:154. https://doi.org/10.1007/s10404-017-1993-5

Gupta A, Magaud P, Lafforgue C, Abbas M (2018) Conditional stability of particle alignment in finite-Reynolds-number channel flow. Phys Rev Fluids 3:1–19. https://doi.org/10.1103/PhysRevFluids.3.114302

Humphry KJ, Kulkarni PM, Weitz DA et al (2010) Axial and lateral particle ordering in finite Reynolds number channel flows. Phys Fluids 22:81703

Hur SC, Tse HTK, Di Carlo D (2010) Sheathless inertial cell ordering for extreme throughput flow cytometry. Lab Chip 10:274–280. https://doi.org/10.1039/b919495a

Kahkeshani S, Haddadi H, Di Carlo D (2015) Preferred interparticle spacings in trains of particles in inertial microchannel flows. J Fluid Mech 786:R3. https://doi.org/10.1017/jfm.2015.678

Kang K, Lee SS, Hyun K et al (2013) DNA-based highly tunable particle focuser. Nat Commun 4:1–8. https://doi.org/10.1038/ncomms3567

Kim JA, Lee JR, Je TJ et al (2018) Size-dependent inertial focusing position shift and particle separations in triangular microchannels. Anal Chem 90:1827–1835. https://doi.org/10.1021/acs.analchem.7b03851

Lagus TP, Edd JF (2012) High throughput single-cell and multiple-cell micro-encapsulation. J Vis Exp 64:e4096. https://doi.org/10.3791/4096

Lagus TP, Edd JF (2013a) High-throughput co-encapsulation of self-ordered cell trains: cell pair interactions in microdroplets. RSC Adv 3:20512–20522. https://doi.org/10.1039/c3ra43624a

Lagus TP, Edd JF (2013b) High-throughput co-encapsulation of self-ordered cell trains: cell pair interactions in microdroplets. RSC Adv 3:20512–20522. https://doi.org/10.1039/c3ra43624a

Lee W, Amini H, Stone HA, Di Carlo D (2010) Dynamic self-assembly and control of microfluidic particle crystals. Proc Natl Acad Sci 107:22413–22418. https://doi.org/10.1073/pnas.1010297107

Lim EJ, Ober TJ, Edd JF et al (2014) Inertio-elastic focusing of bioparticles in microchannels at high throughput. Nat Commun 5:1–9. https://doi.org/10.1038/ncomms5120

Loudon C, Tordesillas A (1998) The use of the dimensionless Womersley number to characterize the unsteady nature of internal flow. J Theor Biol 191:63–78. https://doi.org/10.1006/jtbi.1997.0564

Martel JM, Toner M (2014) Inertial focusing in microfluidics. Annu Rev Biomed Eng 16:371–396. https://doi.org/10.1146/annurev-bioeng-121813-120704

Matas JP, Glezer V, Guazzelli É, Morris JF (2004) Trains of particles in finite-Reynolds-number pipe flow. Phys Fluids 16:4192–4195. https://doi.org/10.1063/1.1791460

Mikulencak DR, Morris JF (2004) Stationary shear flow around fixed and free bodies at finite Reynolds number. J Fluid Mech 520:215–242

Moon HS, Je K, Min JW et al (2018) Inertial-ordering-assisted droplet microfluidics for high-throughput single-cell RNA-sequencing. Lab Chip 18:775–784. https://doi.org/10.1039/c7lc01284e

Morris JF (2001) Anomalous migration in simulated oscillatory pressure-driven flow of a concentrated suspension. Phys Fluids 13:2457–2462. https://doi.org/10.1063/1.1390363

Mukherjee P, Wang X, Zhou J, Papautsky I (2019) Single stream inertial focusing in low aspect-ratio triangular microchannels. Lab Chip 19:147–157. https://doi.org/10.1039/c8lc00973b

Mutlu BR, Edd JF, Toner M (2018) Oscillatory inertial focusing in infinite microchannels. Proc Natl Acad Sci 115:7682–7687. https://doi.org/10.1073/pnas.1721420115

Ozkumur E, Shah AM, Ciciliano JC et al (2013) Inertial focusing for tumor antigen-dependent and -independent sorting of rare circulating tumor cells. Sci Transl Med 5:179ra47. https://doi.org/10.1126/scitranslmed.3005616

Pan Z, Zhang R, Yuan C, Wu H (2018) Direct measurement of micro-scale flow structures induced by inertial focusing of single particle and particle trains in a confined microchannel. Phys Fluids. https://doi.org/10.1063/1.5048478

Reece AE, Oakeya J (2016) Long-range forces affecting equilibrium inertial focusing behavior in straight high aspect ratio microfluidic channels. Phys Fluids 28:043303. https://doi.org/10.1063/1.4946829

Segré G, Silberberg A (1961) Radial particle displacements in poiseuille flow of suspensions. Nature 189:209–210. https://doi.org/10.1038/189209a0

Shen S, Ma C, Zhao L et al (2014) High-throughput rare cell separation from blood samples using steric hindrance and inertial microfluidics. Lab Chip 14:2525–2538. https://doi.org/10.1039/c3lc51384j

Syed MS, Rafeie M, Vandamme D et al (2017) Selective separation of microalgae cells using inertial microfluidics. Bioresour Technol 252:91–99. https://doi.org/10.1016/j.biortech.2017.12.065

Yang S, Kim JY, Lee SJ et al (2011) Sheathless elasto-inertial particle focusing and continuous separation in a straight rectangular

microchannel. Lab Chip 11:266–273. https://doi.org/10.1039/c0lc00102c

Yuan C, Pan Z, Wu H (2018) Inertial migration of single particle in a square microchannel over wide ranges of *Re* and particle sizes. Microfluid Nanofluidics 22:1–13. https://doi.org/10.1007/s10404-018-2120-y

Zurita-Gotor M, Blawzdziewicz J, Wajnryb E (2007) Swapping trajectories: a new wall-induced cross-streamline particle migration mechanism in a dilute suspension of spheres. J Fluid Mech 592:447–469. https://doi.org/10.1017/S0022112007008701